

Assessment of ocean circulation characteristics off the west coast of Ireland using HF radar

Lei Ren^{1,2}, Guangwei Pan¹, Lingna Yang¹, Yaqi Wang¹, Gang Zheng³, Peng Yao⁴, Qin Zhu⁵, Zhenchang Zhu^{5,6,*}, Michael Hartnett⁷

¹ School of Ocean Engineering and Technology, Sun Yat-sen University, Zhuhai, China

² Southern Marine Science and Engineering Guangdong Laboratory (Zhuhai), Zhuhai, China

³ The State Key Laboratory of Satellite Ocean Environment Dynamics, Second Institute of Oceanography, Ministry of Natural Resources, Hangzhou, China

⁴ The National Key Laboratory of Water Disaster Prevention, Hohai University

⁵ Southern Marine Science and Engineering Guangdong Laboratory (Guangzhou), Guangzhou 511458, China

⁶ Guangdong Provincial Key Laboratory of Water Quality Improvement and Ecological Restoration for Watersheds, Institute of Environmental and Ecological Engineering, Guangdong University of Technology, Guangzhou 510006, China

⁷ University of Galway, Galway, Ireland

* Correspondence: zhenchang.zhu@gdut.edu.cn

Abstract: Research on coastal ocean circulation pattern over long time periods is significant for various marine endeavors, such as: environmental protection, coastal engineering construction and marine renewable energy extraction. Based on sea surface current data remotely observed by a shore-based high frequency radar (HFR) system for one year (2016), spatiotemporal characteristics of surface flow fields of sea surface flow fields along the west coast of Ireland are studied using harmonic analysis, rotary spectral analysis and representative flow fields over different seasons and the whole year. Coastal surface currents in the study area are dominantly affected by tidal dynamics of the M2 constituent, showing significant characteristics of regular semidiurnal tide such as M2 and S2. The energy spectrum distribution indicates that the tidal constituents M2 and S2 are the dominant periodic energy constituents in a counterclockwise spectrum, which mainly presents rotating flow; the representative diurnal tidal constituents is the constituent K1, and its energy spectrum distribution is mainly clockwise. A comparison between Probable Maximum Current Velocity (PMCV) and Measured Maximum Current Velocity (MMCV) is presented. It shows that, although tidal current characteristics in the study area are significant, the main driving force of the currents at the time of the maximum currents is wind energy. These results provide new insights into a region of huge societal potential at early stages of sustainable economic exploitation where little data currently exists.

Keywords: high frequency radar; tidal currents; rotational spectral analysis; surface currents; harmonic analysis; maximum ocean currents

Citation: To be added by editorial staff during production.

Academic Editor: Firstname Last-name

Received: date

Revised: date

Accepted: date

Published: date



Copyright: © 2023 by the authors. Submitted for possible open access publication under the terms and conditions of the Creative Commons Attribution (CC BY) license (<https://creativecommons.org/licenses/by/4.0/>).

1. Introduction

Ocean currents are driven by several forces, such as tides, density gradients, wind stress and geostrophic deflection force [1]. Understanding ocean currents is fundamental to a diverse range of marine activities[2]. Therefore, acquiring ocean current data with fine temporal and spatial resolution over a long time to analyze the mechanisms of its movement is important. However, oceanic states are complex processes, and it is difficult to obtain continuous data over a long time relying only on conventional equipment[3].

Conventional ocean current measuring instruments, such as current recorders and Acoustic Doppler Current Profilers (ADCP) measure data at single points. High Frequency Radars (HFR) were developed as an alternative for measuring surface currents at higher temporal and spatial resolutions: HFR is the now widely applied[4-6]. HFR can provide highly resolved temporal (tens of minutes) and spatial data vital to understand marine mechanisms over relatively large domains[7]. These HFR-derived ocean surface currents are utilized at multiple spatiotemporal scales along the coastal regions to understand the spatial variability of tidal currents [8-10]and associated mechanisms[4,7], to investigate the mesoscale and sub-mesoscale eddy dynamics[6,10-12], to understand the coastal upwelling features[13,14] and to unveil seasonal surface circulation variability[5,15-17]. Several radar systems are now widely applied, such as Seasonde CODAR, WERA, and OSMAR. They can be categorized into beam forming and direction-finding types. Beam forming HFR systems electronically steer a linear phased array of receiving antennas toward a sector of ocean surface, such as OSCR and WERA [18,19]. While direction finding HFR system exploits the directional properties of loop antennas to determine bearing, such as CODAR [20].

Regular semidiurnal tides are important and interactions between tide and bathymetry occur over different ranges of depth. Shen, *et al.* [21] conducted a study on the spatial distribution of surface tidal currents in southwestern Taiwan based on HFR dataset using the method of quasi harmonic analysis. They found that tidal currents were affected by semi-diurnal and shallow tidal water constituents. Shallow water tidal constituents are also highly significant off west coast Ireland and are investigated herein. Many processes can benefit from knowledge of the maximum currents in a region, these can be assessed in a number of ways, such as probable maximum current velocity (PMCV) and measured maximum current velocity (MMCV). These currents are particularly relevant to offshore engineering projects, such as the Green Atlantic Project. In this research, remote sensing HFR was used to determine the surface circulation of a proposed large offshore floating wind farm site. Surface currents measured using HFR network during the period December 2015 to December 2016 were analyzed. In order to study the spatiotemporal distribution characteristics and variations of ocean current flows off the western coast of Ireland, we have looked at seasonal variations, significance of wind impacts, tidal ellipses, rotational spectral analysis and maximum current analysis. This is important research as it provides new insights into a region of huge societal potential at early stages of sustainable economic exploitation; when this installation is completed, 1400MW power will be generated from hundreds of floating wind turbines. This electricity will be used to power the national grid through the development of the largest synchronous compensator in the world.

The structure of this paper is as follows. Section 2 presents methodologies, including the study area, HFR system and tide. Results are presented in Section 3. Discussions and main conclusions are given in Section 4.

2. Methodologies

2.1. Study area

Located on the northwest European Continental Shelf, the waters off the Irish west coast span the transitional zone of oceanic to coastal waters, exhibiting characteristics of both coastal and Atlantic behaviour. The width of the continental shelf (defined by the 200 m contour) approaches within 100 km of the coast in the region. In general, the seabed slopes rapidly to 80–100 m within 20 km of the coast, from here the bathymetry plateaus out to the shelf break. Thus shoaling is significant and shallow water tidal constituents contribute to the hydrodynamics of the region. The Atlantic weather systems strongly influence the region; average wind speeds in January are in the order of 11m/s, and during June the average is around 7 m/s [22]. Consequently, wind plays a significant role in de-

termining residual currents circulation in the region [23,24]. The meteorological conditions exert significant influence on magnitudes and directions of surface currents locally; surface currents generally contain contributions from wind stress, whereas winter surface currents may actually be dominated by wind forcing in the study area [25]. Oceanographic data for west coast Ireland is sparse. McMahon et al. [22] described some oceanographic features of the region. A major feature of Ireland's western continental shelf is a thermohaline front, which separates Ireland's coastal waters from offshore waters.

This study focuses on analyses of sea surface currents observed by a HFR system from a full continuous year's data; the system covered an offshore area with maximum meridional and latitudinal lengths of approximately 100 km and 90 km, (see Figure 1 (b)). To ensure reliability and integrity of the dataset, sea surface currents monitored for more than 80% of the observation period were considered monitoring high density points (in total 162) (see Figure 1 (b)). This data selection criterion is the same as that used by Liu, Zhou and Wen [6]. The maximum latitudinal length and meridional lengths of the high-density monitoring area are approximately 40 km and 50 km, respectively. Figure 1 (b) shows that the majority of the high-density points are distributed in the intersection area between two HFR stations.

Observational datasets include: surface currents obtained from the HFR system and tidal water elevations from a tidal gauge close to study area. Detailed descriptions of each dataset are presented below.

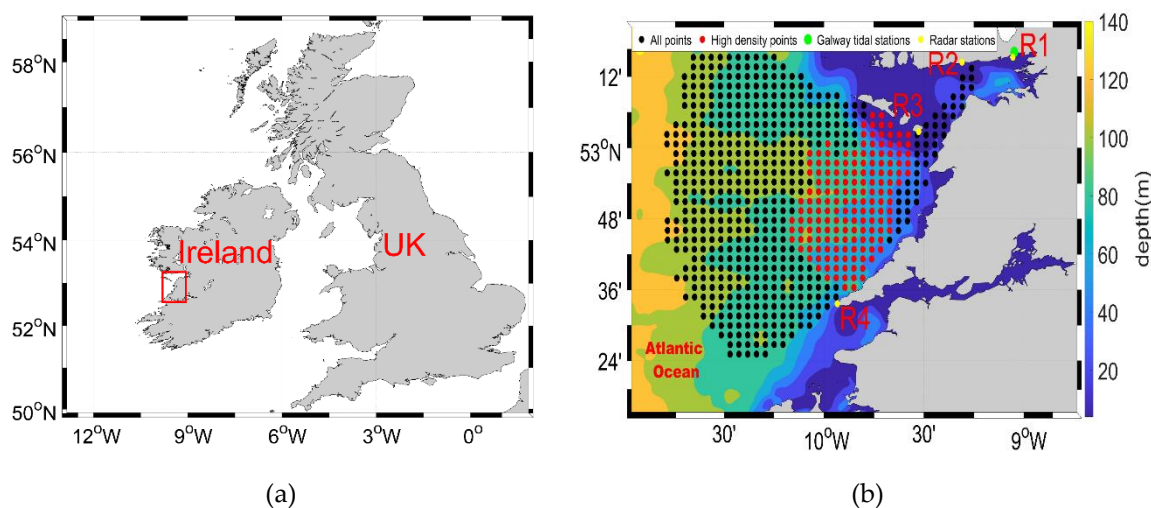


Fig. 1 Study area and data area. (a) location of study area; (b) HFR coverage area and radar sites.

2.2. HFR system

Despite the potential for economic development off the Irish west coast, little commercial exploitation has taken place. Large oil and gas deposits are known to exist on the continental shelf. The region is rich in sea life and has large economic potential for fishing and aquaculture. Studies undertaken in recent years have identified west coast Ireland as being in one of the regions with the highest offshore wind and wave energy potentials in the world [26]. In April 2021 the Irish National Electricity Supply Board (ESB) announced detailed plans to immediately begin the development of a 1.4 GW offshore floating wind farm in the region. This development, Green Atlantic, will include a major hydrogen production facility to store excess wind energy. Post completion, Ireland will become an exporter of clean energy and will benefit significantly in economics terms from this development.

The study area is located on the west coast of Ireland (9.26°–10.79° W, 52.33°–53.26°N), as is shown for the Atlantic in Figure 1. It is located in the westerlies and ocean current movements are affected by the North Atlantic Oscillation and low-pressure system [27,28]. Figure 1 (b) shows that the bathymetry in the study area ranges from 0–140 m, and the isobaths nearshore are roughly parallel to the coastline. To the west of the

study area, the water depth increases suddenly up to approximately 1000m deep ocean waters. The region with depths of 80~100m consists of alternating ridges and troughs. Ridges scattered in the northwest of the study area between 80m and 100m isobaths and to the west of study area with 120m isobaths. This complex bathymetry with ridges, troughs, and basins leads to rapid changes in water depth in the study area. Figure 1(b) also shows the deployment location of HFR stations (R1- R4) and their area of coverage.

HFR is a shore-based sea state monitoring system. Compared with traditional current measuring instruments, it has several advantages: high spatial and temporal resolution, wide area of coverage and it is an all-weather system. HFR senses fields of sea surface currents, waves and sea surface winds using Bragg scattering and Doppler frequency shift effect produced by the interactions between high frequency radio waves and the sea surface [27,29].

The University of Galway deployed two Seasonal HFR stations on Galway Bay in 2011. The four observation stations were connected at the end of 2014, monitoring parameters within approximately 200km of the west coast of Ireland. Characteristics of the radar stations are presented in Table 1. Surface currents monitored by the HFR system over a complete year (December 2015 to December 2016) were selected for this research. Herein, the authors focused on analyzing spatial and temporal characteristics of the surface flow fields with high coverage density.

Inter-comparison between surface currents observed by HFR and ADCP at Galway Bay had been undertaken by O'Donncha, *et al.* [30]. The accuracy of HFR data, with root mean squared error (RMSE) by 10-12 cm/s, was comparable to datasets in other coastal areas, such as surface currents at the southeast of China and currents on Monterey Bay located on the west coast of the USA [6,31].

Table 1. Summary of CODAR HFR system parameters.

Station	Operating frequency (MHz)	Transmitted bandwidth (KHz)	Spatial resolution (km)	Temporal resolution (minutes)	Data averaging period (minutes)
R1	26.425	499.88	0.3	60	94
R2	24.64	499.88	0.3	60	94
R3	13.5	49.63	3	60	75
R4	13.5	49.63	3	60	75

2.3. Tidal current analysis

2.3.1 Tidal current patterns

To investigate tidal hydrodynamics, the major semi-diurnal constituents (M2, S2, and N2), major diurnal constituents (K1 and O1) and shallow water constituents (M4, M6, S4 and MS4) are considered in this study. The major and minor axes of tidal ellipses are determined by the tidal current harmonic constant, and the major axis points in the direction of the maximum velocity of the tidal constituents [32].

A coefficient F is used to describe characteristics of tidal ellipses and tidal currents. Tidal current patterns were assessed using [33]:

$$F = \frac{W_{O1} + W_{K1}}{W_{M2}} \quad (1)$$

where W_{O1} , W_{K1} and W_{M2} are the lengths of the semi-major axes of the tidal ellipses of O1, K1 and M2, respectively.

When $F \leq 0.5$ the area is mainly affected by regular semi diurnal tidal currents; when $0.5 < F \leq 2$ the area is mainly affected by irregular semi diurnal tidal currents; when $2 < F$

≤ 4 the area is mainly affected by irregular diurnal tides; and when $F > 4$ the area is affected by regular diurnal tides [33].

Rotational characteristics of tidal currents can be expressed by the rotation rate R [33]:

$$R = \frac{M_i}{M_a} \quad (2)$$

where M_i is the magnitude of the short axis of its tidal ellipse, and M_a is the magnitude of the major axis of the tidal ellipse.

When the absolute value of the rotation rate R is greater than 0.25 the tidal current has strong rotational flows; when the absolute value of R is less than 0.25, it indicates that the tidal current is characteristic of reciprocating flows. The positive or negative value of R indicates direction of tidal ellipse rotation. When R value is positive, the tidal ellipse moves counterclockwise; when R value is negative, the tidal ellipse moves clockwise [33].

To explore spatial characteristics of tidal currents firstly, surface current data were spatially averaged at each monitoring time [21]. Secondly, harmonic analysis of surface currents was carried out using the t-tide package in Matlab.

2.3.2 Rotary spectral analysis

The Coriolis force is important force to include when analysing ocean currents. Traditional analysis splits an ocean current vector into zonal (u) and meridional components (v). Power spectra of both zonal and meridional components are computed respectively; the direction of ocean current motion is determined from both components. However, traditional methods cannot reflect the action of the Coriolis force, or the influence of the earth's rotation on sea water while analysing the movement of sea surface currents [34-36].

In order to study frequency characteristics of ocean current movements, the methods of spectrum analysis are used in characterizing features of different high frequency dependent data. Rotary spectra, which consider movement of ocean currents as a function of $u(t)$ and $v(t)$ and reflect effect of rotation, have been widely used to analyze the characteristics of currents movements[37,38]. The rotary spectral analysis method is an effective way to determine the strength of different periodic signals in ocean currents motion, and may be used to determine the significance of each tidal constituent.

Here, the rotary spectral analysis method is used to analyze ocean current energy[37,39,40]. Firstly we define current vectors in complex form as [39]:

$$\omega(t) = u(t) + i*v(t) \quad (3)$$

The counterclockwise rotation energy spectrum is defined as:

$$S_+(f) = S_{UU}(f) + S_{VV}(f) + 2\text{Im}[S_{UV}(f)] \quad (4)$$

The clockwise rotation energy spectrum is defined as:

$$S_-(f) = S_{UU}(f) + S_{VV}(f) - 2\text{Im}[S_{UV}(f)] \quad (5)$$

The total energy spectrum S is given by:

$$S = S_-(f) + S_+(f) \quad (6)$$

$$\omega(t) = \frac{1}{2\pi} \int_{-\infty}^{+\infty} e^{i\omega t} dW(f) \quad (7)$$

$$S_{UU}(f) = \frac{1}{2\pi} E \frac{|dW(f)|^2}{d(f)} \quad (8)$$

$$S_{VV}(f) = \frac{1}{2\pi} E \frac{|dW(f)|^2}{d(f)} \quad (9)$$

where $S_+(f)$ and $S_-(f)$ indicates counterclockwise and clockwise rotary spectral respectively; $\omega(t)$ indicates the motion of current vector with time, $u(t)$ represents the motion process of the east component of the surface current vector, $v(t)$ indicates the motion process of northern component of the surface current vector, $S_{UU}(f)$ and $S_{VV}(f)$ represent the auto spectra of $u(t)$ and $v(t)$, respectively. $S_{UV}(f)$ indicates the cross spectrum of $u(t)$ and $v(t)$, Im indicates imaginary part of variable, $W(f)$ represents the Fourier-Stepian transformation of $\omega(t)$, E represents expectation, the increment $dW(f)$ represents the complex amplitude associated with the differential of the circular frequency f [34–36].

The rotary spectral method categorizes the total density spectrum into a clockwise spectrum and a counterclockwise spectrum. The difference spectrum, computed by differentiating the clockwise spectrum with the counterclockwise spectrum, can be used as an important index to evaluate patterns of ocean flow vectors. If the value of the difference spectrum is 0, it indicates absolute reciprocating motion of the current on a line segment and the rotation coefficient of the current vector is 0 [34–36]. The absolute value of the rotation rate is the ratio of the differential spectral energy density to the total spectral energy density. If the rotation rate of the current vectors is 1, then the current vector is in complete rotational motion [35].

In this research, the hourly surface current data over the year 2016 obtained from HFR observation system were analyzed as follows. Firstly, since few gaps exist among the observations, missing data for observational points with high coverage density were filled using linear interpolation, a commonly used approach in data filling. Secondly, surface currents were averaged in space. Thirdly, the spatially-averaged surface current dataset was used for rotary spectral analysis.

2.3.3. Effects of bathymetry variation on currents

Marine bathymetry influences shallow water constituents of tidal currents. The coefficient of shallow tidal water constituent, G , is used to describe effects of bathymetry in tidal wave propagation and the movements of tidal currents; G is calculated as follows [33]:

$$G = \frac{W_{M4} + W_{MS4}}{W_{M2}} \quad (10)$$

where W_{M4} is the major axis of the M4 tidal ellipse, W_{MS4} is the major axis of MS4 tidal ellipse, and W_{M2} is the major axis of the M2 tidal ellipse.

G describes the influence of bathymetry on the propagation of a tidal wave. When G is greater than 0.04 the effect of the shallow tidal water constituent is considered significant. The higher the value of G , the more significant the effect of coefficient of shallow tidal water constituents [33].

2.4. Maximum ocean currents

In order to study the main driving force of surface current movement at some particular time, the time of maximum ocean current was selected. PMCV and MMCV are widely used in the field of marine engineering, the comparison between PMCV and MMCV is often used to study whether wind or tidal forces dominate the movements of ocean currents at the time of the maximum current speeds. PMCV is an estimated vectors of the maximum current speeds based on the outcome of harmonic tidal analysis. MMCV is a measured vector of the maximum current speeds, in this case based on HFR observations. MMCV represents extreme current speed at each spatial point during the analysis period [33]. Values of PMCV can be obtained from:

$$\vec{PMCV} = 1.29 \times \vec{W}_{M2} + 1.23 \times \vec{W}_{S2} + \vec{W}_{O1} + \vec{W}_{K1} \quad (11)$$

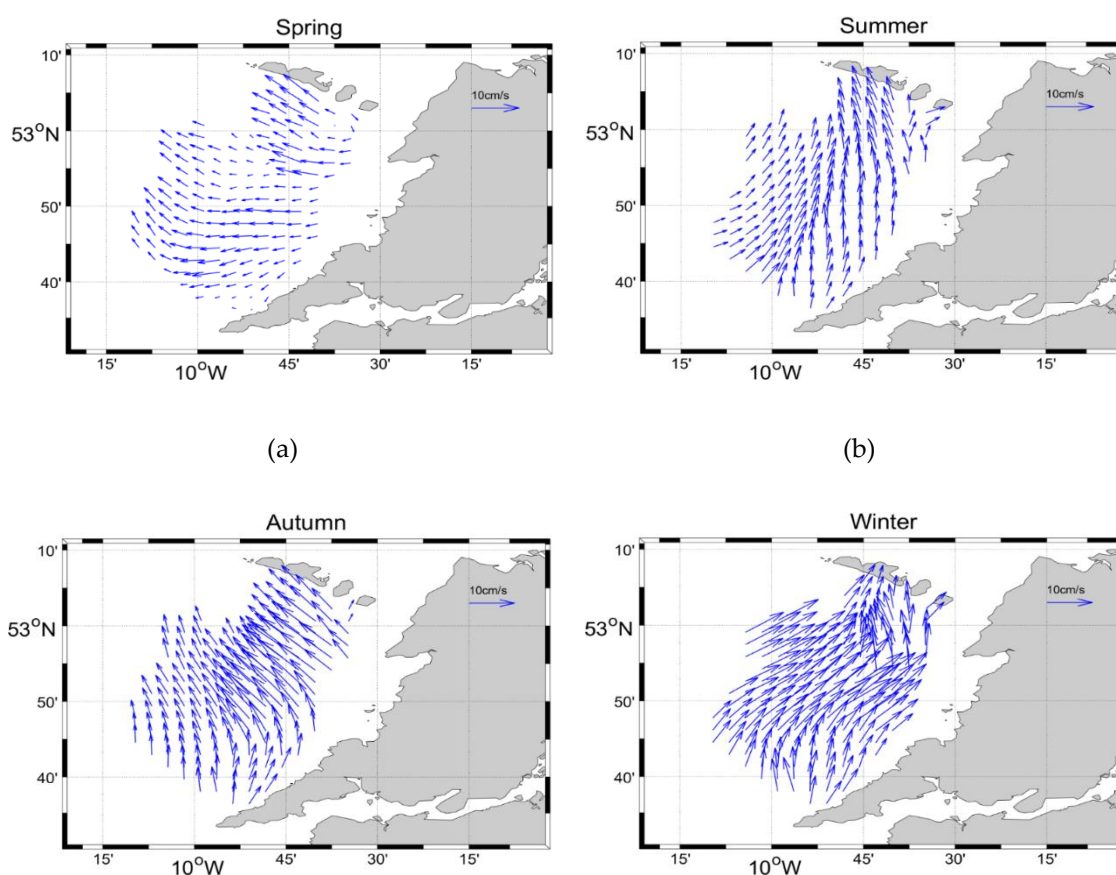
where \vec{W}_{M2} , \vec{W}_{S2} , \vec{W}_{O1} , \vec{W}_{K1} represent the semi-major axis vectors of tidal ellipses of M2, S2, O1, K1, respectively.

3. Results

3.1. Mean surface flow fields

To explore the general spatial distribution characteristics of sea surface flow fields in the study area at a seasonal scale, HFR surface currents were averaged at each observation point over a whole year and four seasons separately. Figure 2(a)-(d) show the mean vector maps in spring, summer, autumn and winter, respectively. Figure 2(e) shows the mean surface vector fields over the full analysis year.

Figure 2 shows that flow directions and magnitudes of mean surface vectors are significantly different across the four seasons. Flow directions of mean surface vectors are predominantly northern or western. In spring, the distribution of the mean surface flow field is quite disparate, dominant flow directions are northwestern and western (see Figure 2(a)). However, flow directions of mean surface vectors in summer, autumn, winter and the whole analysis year are more consistent and are mainly northeast and northwest. In summer, the mean surface flows had northwestern directions only near the north of the study area due to the blocking of the islands (see Figure 2(b)). In autumn, the flow trend of mean surface flow field is mainly northwest. Northeastern flow trend only occurred at few points close to the West Atlantic Ocean. Figure 2(d) shows that mean surface flows in winter dominantly had a northeastern flow trend. Only in the northern part of the observation area a northwest flow exists due to the blocking of the northern islands. Figure 2(e) shows that northward flow is the dominant trend of annual mean surface flow fields. The annual mean surface flow field presents a northward flow in the southern part of study area, while northwestern flow trend exists in the northern part. This difference may result from due to the blocking effect of the northern islands (Aran Islands).



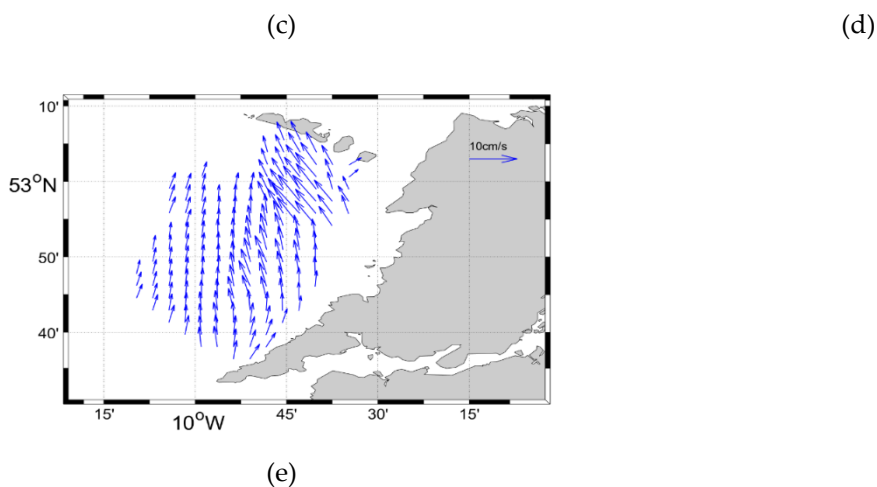


Fig. 2 Mean surface vector fields. (a)–(d) are mean surface flow fields in spring, summer, autumn, and winter, respectively; (e) is mean surface flow fields during the analysis period (year 2016).

To further analyze characteristics of mean flow fields at a seasonal scale, the maximum, minimum and mean values in space are computed; these are presented in Table 3. Table 3 shows that the maximum and minimum values of the time averaged surface current velocity occur in autumn and spring; they are 15.27 cm/s and 0.28 cm/s respectively. The maximum current speed of autumn is approximately twice that of spring. The mean current speed of winter is considerably greater than that of the other seasons; it is nearly twice the annual average speed. The mean value of averaged surface velocity for the full year is less than the values during summer, autumn and winter.

Table 3. Statistics of temporally averaged surface current speeds (cm/s)

Statistics	Spring	Summer	Autumn	Winter	Full Year
Maximum	7.07	9.00	15.27	13.56	10.58
Minimum	0.28	2.78	2.43	5.54	2.92
Mean	3.07	6.01	7.62	9.26	5.54

3.2. Tidal elevation analysis

Tidal water levels from the nearest tidal gauge (Galway port, as is shown in Figure 1(b)) were used for harmonic analysis using MATLAB's t-tide package [41]. Based on the original HFR current data, 67 tidal constituents (with 95% confident interval) were extracted using the method proposed by Halverson and Pawlowicz [42]. Note that only those tidal constituents with signal to noise ratio (SNR) are greater than 2 are considered significant and quantified in this study. The diurnal tidal constituents (K1, O1, P1, Q1), semidiurnal tidal constituents (M2, N2, S2, K2) and shallow tidal water constituents (M4, MS4, M6) are presented in Table 4.

Table 4 shows that M2 and K1 constituents have the maximum amplitudes of the semidiurnal and diurnal constituents respectively. The M2 amplitude is approximately 3 times greater than the S2 constituent, 5 times greater than the N2 constituent and 10 times greater than the K2 constituent. The amplitude of the K1 tidal constituent is approximately 2 times greater than the O1 constituent, and 5 times greater than the Q1 constituent. The averaged amplitudes of the semi-diurnal constituents are approximately 11 times greater than the diurnal constituents and 25 times greater than the shallow tidal water constituents. The values of the amplitudes of different shallow tidal water constituents are similar,

while the amplitudes of diurnal tidal constituents and semi-diurnal tidal constituents are significantly different.

Table 4. Amplitudes and phases of tidal water elevation (December 2015 to December 2016)

Tidal constituent	Amplitude (cm)	Phase (°)	SNR
M2	150.28	125.81	480000.00
S2	54.64	158.05	67000.00
N2	30.87	105.16	25000.00
K2	15.56	156.73	3000.00
K1	10.79	62.82	750.00
O1	7.16	316.71	200.00
M4	3.72	329.77	770.00
P1	3.65	50.61	99.00
MS4	3.19	47.98	580.00
M6	3.11	350.11	120.00
Q1	2.22	265.40	18.00

3.3. Characteristics and patterns of tidal currents

Based on the spatially-averaged sea surface current data, the value of the coefficient F calculated, Equation (1), is 0.3009; this indicates that the tidal currents exhibit strong semi diurnal characteristics. To further study characteristics of tidal currents, harmonic, spectral and tidal ellipses analyses on HFR data were performed and presented in following sections.

3.3.1. Harmonic analysis on spatially-averaged surface currents

The dominant astronomical and shallow water tidal constituents are presented in descending order of amplitude in Table 5. Meteorological tidal constituents SA (solar annual constituent) and SSA (solar semiannual constituent) are determined by solar radiation and other meteorological factors on an annual scale [43]. Since the length of the surface current data analyzed in this research is only one year, it is not possible to undertake an effective analysis of the characteristics of these constituents. Thus, meteorological tidal constituents were not included in this study.

Table 5 shows that amplitude of the M2 tidal constituent is approximately three times and four times greater than of the S2 and N2 constituents respectively. The amplitude of the K1 tidal constituent is approximately equal to the S1 and P1 constituents, and about twice as large as the O1 constituent. The average amplitudes of semi-diurnal tides are approximately three times that of diurnal tidal constituents, and 16 times that of shallow tidal water constituents. The values of the amplitudes of different shallow tidal water constituents are similar to each other, while the amplitudes of diurnal tidal constituents and semi-diurnal constituents are significantly different from each other. Thus the energy of the semi-diurnal signals is dominant in the study area compared with other periodic signals. The value of F here is 0.30 (<0.50), indicating that the tidal surface currents had significant contributions from semidiurnal constituents which is consistent with above.

In addition, Table 5 shows that ocean current movement is significantly affected by the semidiurnal tidal constituents, including M2, S2 and N2; M2 plays a major role. To investigate rotational characteristics of tidal currents, dominant constituents M2 and S2 are selected to calculate rotation rate using, Equation (2). The results show that the rotation rates (R) of M2 and S2 are 0.56 and 0.32 respectively. The absolute value of rotation rates are greater than 0.25, and also their rotation rates are positive; this indicates that the

tidal ellipses of M2 and S2 exhibit rotational flow, and their direction of rotation is predominantly counterclockwise. Additionally, results indicate that the rotationality of the M2 tidal ellipse is more significant than that of the S2 tidal ellipse.

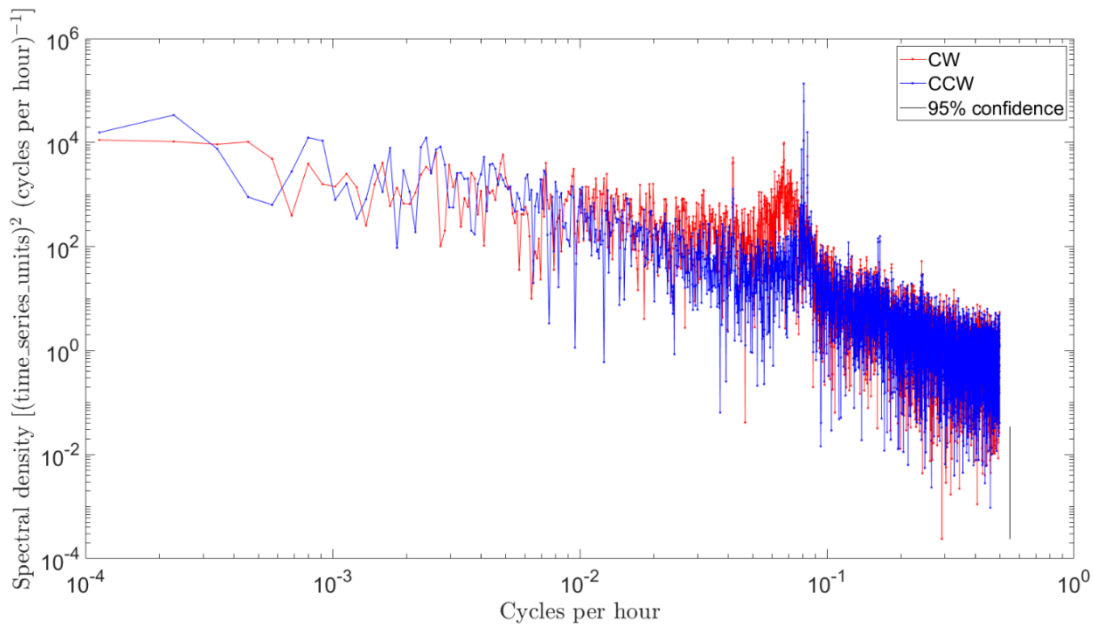
Table 5. Summary of harmonic analysis for spatially-averaged surface currents (December 2015 to December 2016)

Tidal constituent	Amplitude (cm/s)	Phase (°)	Period (hour)
M2	9.5661	264.29	12.42
S2	3.8180	116.11	12.00
N2	2.3696	55.89	12.66
K2	0.8610	128.53	11.97
K1	1.8667	171.11	23.93
S1	1.4701	33.25	24.00
P1	1.4384	126.26	24.07
O1	0.7627	225.74	25.82
M4	0.3683	326.92	6.21
MS4	0.3332	197.86	6.10
M6	0.2629	242.66	4.14

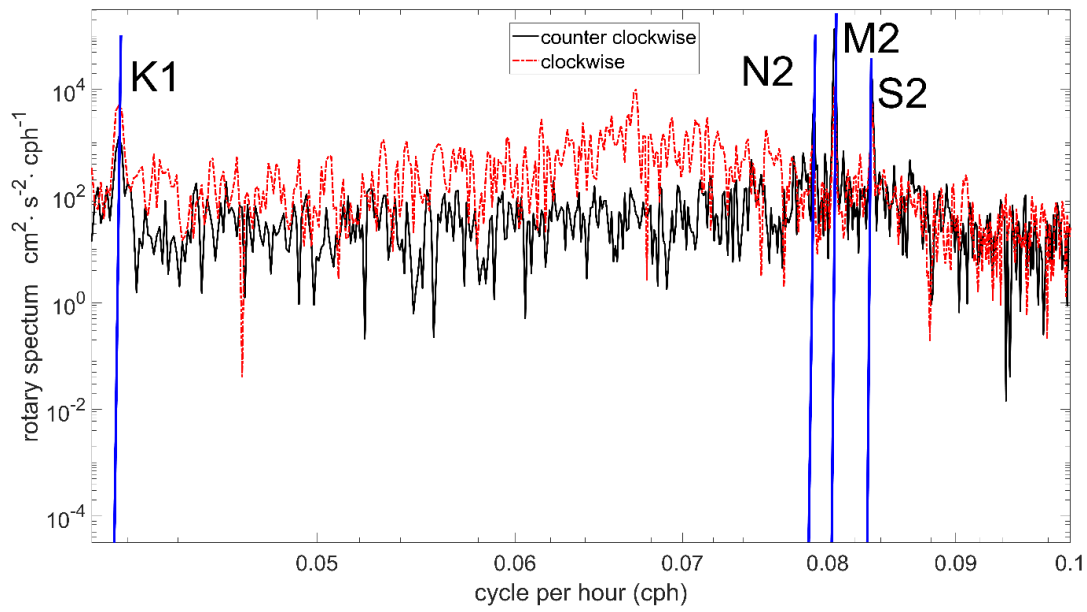
3.3.2 Rotary Spectral Analysis

To further hydrodynamics in the study area, rotational spectral analysis was conducted on spatially averaged surface tidal currents, see Figure 3. Nowhere in the study area did flows exhibit absolute rotational flows. Figure 3(a-b) shows clockwise spectra and counter clockwise spectra of currents and Figure 3(c) shows the total spectrum of currents.

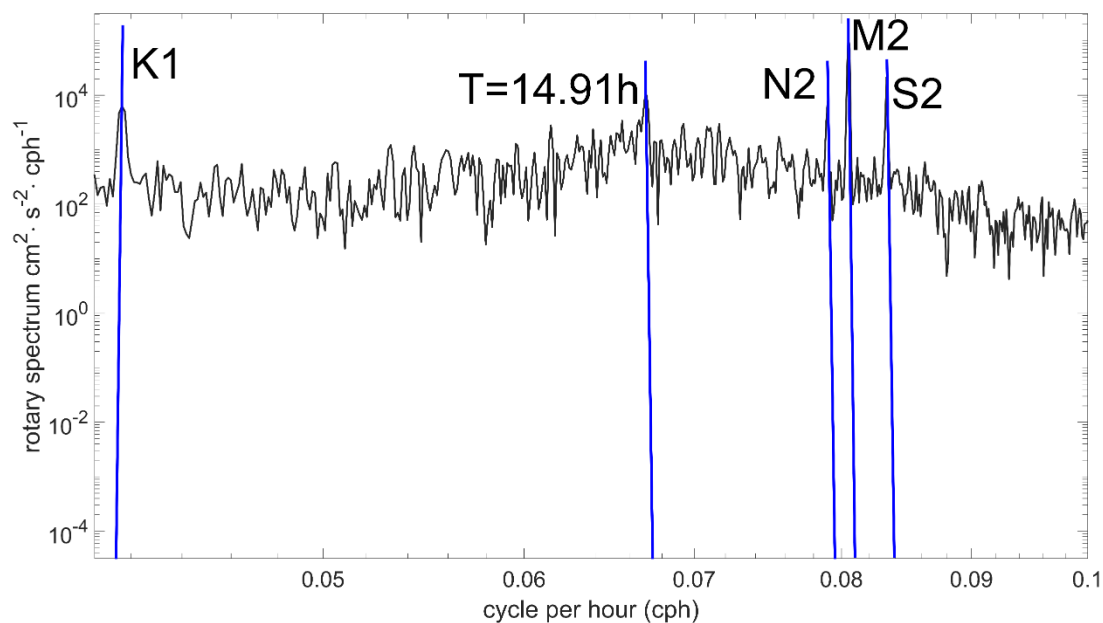
The magnitude of the rotary spectrum is significant in the frequency range 0.03 cph to 0.1 cph; thus rotary spectra in the range 0.03 cph to 0.1 cph is chosen for further analysis, Figure 3(b). Through rotary spectral analysis dominant tidal constituents are chosen to describe variation characteristic of tidal currents. From analysis of the spectra in Figure 3(b), it can be shown that this counterclockwise spectrum of surface currents accounts for 52% (the counterclockwise spectrum at all frequencies/ the total spectrum at all frequencies) of the total spectral energy density; while the clockwise spectrum accounts for the other 48% (the clockwise spectrum at all frequencies/ the total spectrum at all frequencies). 45% of the frequency of the difference spectrum has behaves as a counterclockwise spectrum and 55% of the frequency behaves as a clockwise spectrum. The counterclockwise spectrum accounts for more of the total spectral energy density and less of the of the difference spectrum, this indicates that the counterclockwise density spectrum is dominant in the total energy density spectrum. However, the frequency distribution of the counterclockwise density spectrum is relatively concentrated; the spectrum peaks are concentrated in a relatively narrow frequency range, while the clockwise density spectrum is dispersed over a broader frequency range. The energy density of the clockwise spectrum is higher than that of the counterclockwise spectrum in most frequencies. The energy density of the semidiurnal tidal constituents, dominated by M2 and S2, accounts for 16% of the total spectral energy. The counterclockwise energy density of the frequency corresponding to the M2 tidal constituent accounts for 13%. In combination with analysis of Figure 3(c), counterclockwise energy spectrum of semidiurnal constituents, especially M2, contributes the most to the total energy spectrum. Spectral energy presents a cusp around 0.067 cph (cycle per hour) in Figure 3, which corresponds to the period of inertial flow in study area.



(a)



(b)



(c)

Fig. 3 Clockwise and counter clockwise rotational power spectra (December 2015 to December 2016). 377
 (a) entire spectra; (b) spectra in frequency range of interest; (c) total rotational power spectrum. 378

Analysis of tidal patterns and rotary spectra indicates that the pattern of tidal currents in the study area is mainly driven by semi-diurnal tidal forcing. The range of low frequency corresponds to the period of one year, half a year and several months. The spectral peak density may be affected by wind stress, showing strong monthly and seasonal characteristics. 379
 380
 381
 382
 383

3.3.3. Spatiotemporal rotation of surface currents 384

To further investigate the characteristics of tidal currents movement, the spatial distribution of tidal ellipses is analyzed as shown in Figure 4. Based on the harmonic analysis of the HFR surface currents and tidal water elevations at Galway port, M2 and S2 (astronomical constituents) tidal ellipses are shown in Figure 4. According to the rotary spectral analysis, the energy density of M2 tidal constituent accounts for the highest proportion of all constituents. In the high-density coverage area, the major and minor axes of the M2 tidal ellipses are generally larger than those of the S2 tidal constituent. The average lengths of major and minor axes of M2 tidal ellipses are 9.51 cm/s and 4.47 cm/s, respectively; the average lengths of major and minor axes of S2 tidal ellipses are 3.70 cm/s and 1.14 cm/s, respectively. The mean lengths of the major and minor axes for M2 tidal ellipses are approximately 3 to 4 times greater than those of S2 tidal ellipses. This indicates that the effect of the M2 constituent on tidal currents was more significant than that of the S2 constituent. For the semidiurnal tidal signals, M2 and S2, most of the current ellipses mainly exhibit counterclockwise flow, only one tidal ellipse of M2 is in a clockwise direction; this ellipse is located in the southeast region of the study area. The tidal ellipses of the S2 constituent exhibit counterclockwise flow over the entire study area. 385
 386
 387
 388
 389
 390
 391
 392
 393
 394
 395
 396
 397
 398
 399
 400

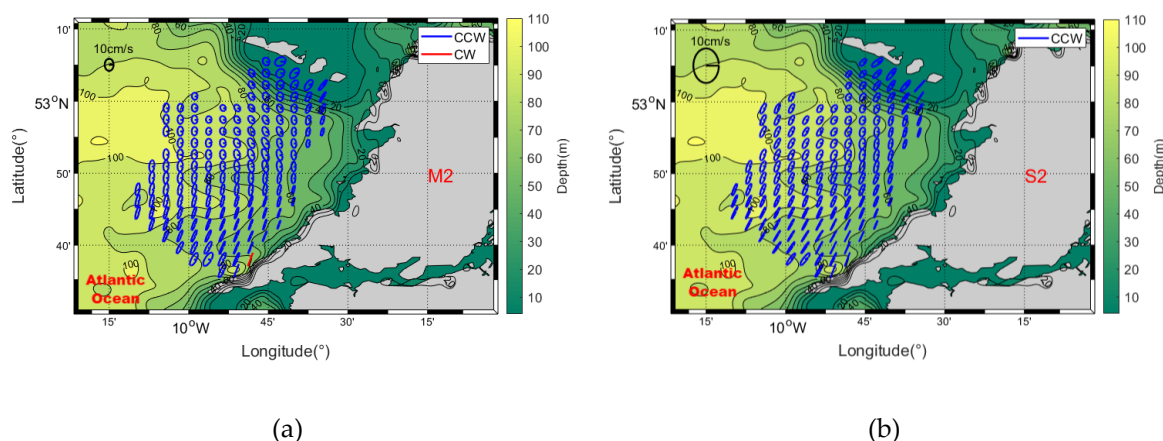


Fig. 4 Tidal ellipses for (a) M2 constituent and (b) S2 constituent (CW means clock wise, CCW means counter clockwise). Note. Scales are different in Figures 4(a) and 4(b).

M2 and S2 tidal ellipses mainly exhibit rotating flow, the rotation of M2 ellipses are more pronounced than those of S2 ellipses. As shown in Figure 4(a), the M2 tidal ellipses in the northwest of the study area tend to rotate flow whereas the tidal ellipses in the southeast of study area, exhibit reciprocating flow tendency. The spatial distribution characteristics of tidal ellipses of both S2 and M2 are similar. They show the characteristics of rotating flow in the northwest of the study area, and more reciprocating flow characteristics in the southeast direction due to topographic steering. Although S2 ellipses generally exhibit rotating flow, the rotational characteristics are not as pronounced as the M2 ellipses. Considering the two dominant tidal ellipses, their flow structures are influenced by both coastal topography and submarine bathymetry. The tidal ellipses in the north-west of the study area exhibit rotational flow tendencies since they are less affected by the islands; while the tidal ellipses in the east of the study area are inclined to show reciprocating trends because they are more affected by coastal topography.

However, the tidal ellipses in the south of the study area show that reciprocating flow characteristics are not related to distance from the coast. This is due to the block of coastal topography in the movements of sea surface currents. The reciprocating flows are due to both coastal topography and submarine bathymetry. Sea surface currents in the area of seabed ridges tend to show reciprocating characteristics while the currents in the area of seabed slopes show rotational characteristics; this explains why currents in the north of the study show rotational characteristics despite proximity to the islands and explains why sea surface currents in the south show reciprocating characteristics in the area of seabed ridges regardless of distance from the coast.

In the middle of the study area, bathymetry slope changes slowly compared with the northern and southern part of the study area. Offshore tidal ellipses (west of the study area) exhibit reciprocating flow tendencies while tidal ellipses close to shore (east of the study area) exhibit rotating flow tendencies. However, tidal ellipses exhibit reciprocating flow tendencies in the northern and southern part of study area because of energy propagating caused by significant bathymetric slope changes.

A clockwise spectrum represents energy propagating from top to bottom; and an anticlockwise spectrum represents energy propagating from bottom to top [11,37,44]. Surface current tidal ellipses are affected by variations in submarine bathymetry because these variations influence vertical energy propagation, a factor which controls movements of tidal ellipses.

The shallow tidal water constituent is a kind of tidal constituent caused by abrupt change in water depth when a tidal wave propagates from deep sea to shallow water. The shallow tidal water constituent coefficient based on M4, MS4 and M2 tidal constituents

can be used to characterize the influence of how the marine topography in an area affects propagation of a tidal wave. Comparison between water depths and the distribution of the coefficients of shallow tidal water constituents at high density points (see Figure 5) shows that areas with small coefficient of shallow tidal water constituents correspond to seabed areas with shallow slopes. Conversely, areas with large coefficient of shallow tidal water constituents are mainly located in areas with significant bathymetric changes. Iso-lines of the coefficients of shallow tidal water constituents are not parallel to the coastline or adjacent isobaths as basin bathymetry has characteristics of isolated aggregation in these areas. This indicates that there is an abrupt change in water depth at points with high coefficient of shallow tidal water constituents in the south of study area. Two other areas of abrupt change in bathymetry occur in the middle and south of the study area, they are between 60m and 80m isobaths (see Figure 5(a)).

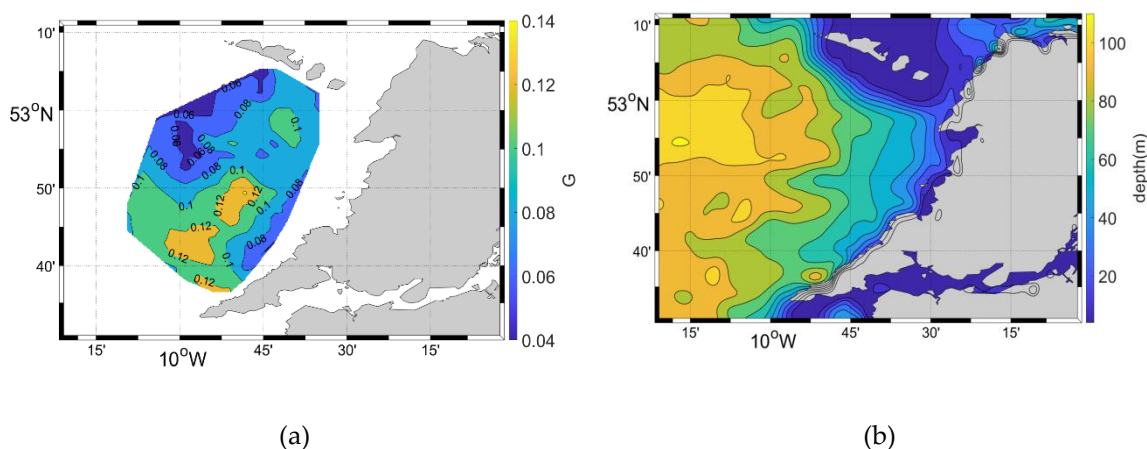
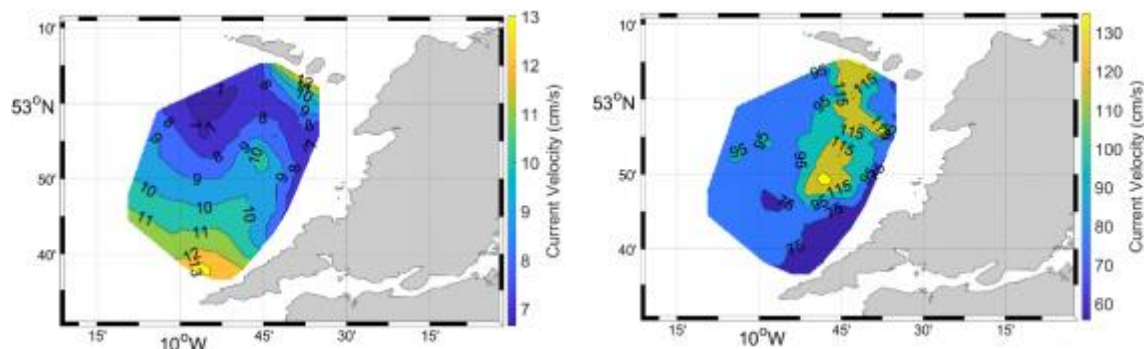


Fig. 5 Comparison between (a) spatial distribution of the coefficient of shallow tidal water constituents (G) and (b) contours of water depth.

The coefficients of shallow tidal water constituent, in this study area are in the order of 0.08 (>0.04), this suggests that the shallow tidal water constituent effect is significant. This is important as it illustrates that, hydrodynamically, this region is in the transition between deep sea and shallower coastal waters and is influenced by this feature. Further, there are a few areas, such as in the south of the study area, with large shallow tidal water constituent coefficients where values are greater than 0.10. These values occur in areas where marine bathymetry was varying more abruptly.

3.4. Characteristics of maximum surface currents maxima

In order to provide useful information for coastal engineering operations and to further study the mechanisms of surface current movements, the maximum surface current velocities, both PMVC and MNCV, were computed using Equation (11); summary results are presented in Figure 6.



(a) (b)

Fig. 6 Comparison between (a) PMCV and (b) MMCV.

Figure 6 shows range and distribution of PMCVs and MMCVs throughout the study area. The ranges of PMCVs and MMCVs are 7 cm/s to 13 cm/s and 60 cm/s to 130 cm/s, respectively; very large differences exist between the 2 velocity fields. Large values of PMCV prevail in the south and north of the region, while large values of MMCV prevail in the center of the region. The spatial distribution of PMCVs does not agree well with that of MMCVs, primarily due to wind influences. To investigate effects of wind on MMCVs, statistics of spatially annually averaged ECMWF wind speeds, maximum, minimum and mean values, are presented in Table 6.

Table 6 shows that the maximum annual wind speed occurs in winter by 21.96m/s. Average wind speeds are the highest (9.03m/s) and least (6.38m/s) in winter and summer respectively. At times of maximum wind speeds, more energy is transferred from the top surface layer of the water column; surface current speeds are highly influenced by strong winds [45]. Wind stresses cause the large differences between PMCV and MMCV.. PMCVs are based on the computation of tidal constituents alone and only reflect tidally driven currents; however, in this region strong prevailing winds significantly increase speeds of surface currents. PMCVs do not correlate well with MMCVs in the study area; our analysis has shown that PMCVs should not be used for estimating maximum surface currents in the region, doing so will result in grossly under-estimated velocities.

Table 6. Statistics of wind speeds

Variable	Statistics	Spring	Summer	Autumn	Winter	Full Year
Wind Speed (m/s)	Maximum	21.31	14.28	18.26	21.96	21.96
	Average	6.64	6.38	7.21	9.03	7.28
	Minimum	0.14	0.13	0.03	0.42	0.03

The above approach presents a most useful methodology to determine significant characteristics of complex oceanographic features. This is the first time these techniques have been applied to a highly wind dominated environment.

4. Discussion

As expected, tidal currents in the study area are shown to be dominated by semi-diurnal constituents especially M2 and S2 tidal constituents. Shallow water tidal constituents are generated by abrupt changes in bathymetry. These constituents give rise to a complex hydrodynamics regime, including changes to slopes of tidal ellipses.

Previously, studies on mechanics of current movements have been undertaken using spectral analysis. Li, *et al.* [46] studied the characteristics of tidal currents in the northern South China Sea using rotational spectral analysis and found the power spectral density is stronger at the diurnal frequency band than at the semidiurnal frequency band. However, the tidal currents in this study are dominated by semidiurnal tides. Li *et al.* [46] studied the characteristics of tidal force over depth, they found that the clockwise spectrum was stronger than the counterclockwise spectrum, and that the counterclockwise spectrum dominated the spectral power density of total rotary spectral. Rotary spectral analysis on HFR surface currents in our study area indicates that the counterclockwise spectrum dominated current movements. Yang, *et al.* [47] found that tidal ellipses around Tangshan International Tourism Island exhibited reciprocating characteristics, whereas tidal ellipses exhibited rotational characteristics in our study area. Additionally, Ren *et al.* [45] studied residual current circulation and its response mechanism to wind at a seasonal

scale for the same area; this study mainly focused on characterizing patterns of tidal currents. Detailed analysis herein of mean surface flow fields, spatially-averaged surface currents and maximum surface currents provide a new perspective when assessing ocean currents.

Shen *et al.* [33] found that the PMCV was in accordance with the MMCV around the Zhoushan Islands; PMCVs and MMCVs exhibit very significant difference in our study area; wind is one of the main driving forces of surface currents at the time of MMCV rather than tidal forcing alone. Because only a one-year dataset was used for analysis in this research, effects of SA and SSA constituents were not considered in detail. Further, differences between PMCVs and MMCVs may also be because the movements of currents at the time of maximum current are mainly driven by meteorologically variable wind rather than tidal force. Thus, in this area it is important not to use the PMCV method when estimating maximum currents. In locations where strong prevailing winds exist, it is very important that MMCVs are determined and PMCVs should not be relied upon to provide estimates of maximum surface currents.

5. Conclusions

Surface currents obtained from HFR system were used to study characteristics of tidal and non-tidal currents of west coast of Ireland island in this research using a rigorous methodology. Characteristics and patterns of tidal currents were analyzed and discussed above. The main conclusions from our research are as follows:

(1) The direction of temporally-averaged flow in the four seasons and over the whole year in the study area shows significant northerly flow. Flow direction of currents in spring and autumn is primarily westerly, the temporally averaged currents in the other three seasons and the whole year show that flow directions are strongly related to wind direction. The surface currents are affected not only by the wind stress, but also steered by bathymetry and topography.

(2) Surface flow fields in the study area are mainly affected by the tidal dynamics of M2 constituent, showing significant regular semidiurnal tide characteristics. The tidal ellipses mainly exhibit rotating flow patterns.

(3) Shallow water tidal constituents are significantly influenced by changes in bathymetry. Values of the coefficient of shallow tidal water constituents are relatively large in areas with abrupt change of bathymetry.

(4) During times of maximum wind speeds, MMCVs are dominated by wind stress, whereas PMCVs are only affected by tidal dynamics. Spatial distributions of differences between MMCVs and PMCVs are very significant. Distributions of PMCVs and MMCVs are not spatially well-correlated throughout the study area. This is because wind is the main driving force of surface currents at the time of MMCV. It is very important that in locations where strong winds prevail that surface maxima are estimated using MMCV rather than PMCV.

Forecasting of surface currents in the study area is going to be carried out in further study using alternative methods such as machine learning methods. Through the analysis of surface currents in the study area, the significant driven factors of the currents will be chosen as inputs to develop prediction models. New information and approach have been presented in this paper that will be significant for the commercial exploitation of marine assets of the west coast of Ireland; also, tracking pollutant slick, such as oil spills, will require highly accurate estimates of surface currents. More ocean current data at depth which are not available during this study should be measured and used in the analysis of the vertical structure of currents in this hydrodynamically complex region.

Author Contributions: Conceptualization, L.R. and G.P.; methodology, G.P.; validation, L.R. and G.P.; formal analysis, G.P., Y.W. and P.Y.; investigation, L.Y. and P.Y.; resources, L.R. and M.H.; data curation, L.R. and M.H.; writing—original draft preparation, L.Y., Y.W., G.Z., Q.Z. and Z.Z.; writing—review and editing, L.R., Z.Z. and M.H.; visualization, G.P., L.Y. and Y.W.; supervision,

L.R.; project administration, L.R., G.Z. and Z.Z; funding acquisition, L.R. and Z.Z. All authors have read and agreed to the published version of the manuscript.

Funding: This work was supported by the Belt and Road Special Foundation of the National Key Laboratory of Water Disaster Prevention [No. 2022ms15]; the Open Research Fund of State Key Laboratory of Estuarine and Coastal Research under Grant [No. SKLEC-KF202103]; the State Key Laboratory of Satellite Ocean Environment Dynamics, Second Institute of Oceanography, MNR and the Zhejiang Provincial Natural Science Foundation of China under Grant [No. LR21D060002].

Data Availability Statement: The data presented in this study are available on request from the corresponding author.

Acknowledgments: We would like to thank ECMWF for providing wind data and the Irish Marine Institute for providing the tidal data.

Conflicts of Interest: The authors declare no conflict of interest.

561
562
563
564
565
566
567
568
569
570
571
572
573

References

1. Capodici, F.; Cosoli, S.; Ciraolo, G.; Nasello, C.; Maltese, A.; Poulain, P.-M.; Drago, A.; Azzopardi, J.; Gauci, A. Validation of HF radar sea surface currents in the Malta-Sicily Channel. *Remote sensing of environment* **2019**, *225*, 65-76. 574-576
2. Hays, G.C. Ocean currents and marine life. *Current Biology* **2017**, *27*, R470-R473. 577
3. Mantovani, C.; Corgnati, L.; Horstmann, J.; Rubio, A.; Reyes, E.; Quentin, C.; Cosoli, S.; Asensio, J.L.; Mader, J.; Griffa, A. Best practices on high frequency radar deployment and operation for ocean current measurement. *Frontiers in Marine Science* **2020**, *7*, 210. 578-580
4. Tran, M.C.; Sentchev, A.; Nguyen, K.C. Multi-scale variability of circulation in the Gulf of Tonkin from remote sensing of surface currents by high-frequency radars. *Ocean Dynamics* **2021**, *71*, 175-194. 581-582
5. Ren, L.; Chu, N.; Hu, Z.; Hartnett, M. Investigations into synoptic spatiotemporal characteristics of coastal upper ocean circulation using high frequency radar data and model output. *Remote Sensing* **2020**, *12*, 2841. 583-584
6. Liu, F.; Zhou, H.; Wen, B. DEDNet: Offshore eddy detection and location with HF radar by deep learning. *Sensors* **2020**, *21*, 126. 585-586
7. Mandal, S.; Sil, S.; Gangopadhyay, A. Tide-current-eddy interaction: A seasonal study using high frequency radar observations along the western Bay of Bengal near 16° N. *Estuarine, Coastal Shelf Science* **2020**, *232*, 106523. 587-588
8. Chavanne, C.; Flament, P.; Carter, G.; Merrifield, M.; Luther, D.; Zaron, E.; Gurgel, K.J.J.o.p.o. The surface expression of semidiurnal internal tides near a strong source at Hawaii. Part I: Observations and numerical predictions. **2010**, *40*, 1155-1179. 589-591
9. Gough, M.K.; Garfield, N.; McPhee - Shaw, E. An analysis of HF radar measured surface currents to determine tidal, wind - forced, and seasonal circulation in the Gulf of the Farallones, California, United States. *Journal of Geophysical Research: Oceans* **2010**, *115*. 592-594
10. Mandal, S.; Sil, S.; Gangopadhyay, A.; Murty, T.; Swain, D. On extracting high-frequency tidal variability from HF radar data in the northwestern Bay of Bengal. *Journal of Operational Oceanography* **2018**, *11*, 65-81. 595-596
11. Mandal, S.; Sil, S.; Pramanik, S.; Arunraj, K.S.; Jena, B.K. Characteristics and evolution of a coastal mesoscale eddy in the Western Bay of Bengal monitored by high-frequency radars. *Dynamics of Atmospheres Oceans* **2019**, *88*, 101107. 597-598
12. Schaeffer, A.; Gramouille, A.; Roughan, M.; Mantovanelli, A. Characterizing frontal eddies along the East Australian Current from HF radar observations. *Journal of Geophysical Research: Oceans* **2017**, *122*, 3964-3980. 599-600
13. Lorente, P.; Piedracoba, S.; Montero, P.; Sotillo, M.G.; Ruiz, M.I.; Álvarez-Fanjul, E. Comparative Analysis of Summer Upwelling and Downwelling Events in NW Spain: A Model-Observations Approach. *Remote Sensing* **2020**, *12*, 2762. 601-602
14. Paduan, J.D.; Cook, M.S.; Tapia, V.M. Patterns of upwelling and relaxation around Monterey Bay based on long-term observations of surface currents from high frequency radar. *Deep Sea Research Part II: Topical Studies in Oceanography* **2018**, *151*, 129-136. 603-605
15. Kohut, J.T.; Glenn, S.M.; Chant, R.J. Seasonal current variability on the New Jersey inner shelf. *Journal of Geophysical Research: Oceans* **2004**, *109*. 606-607
16. Mandal, S.; Sil, S.; Gangopadhyay, A.; Jena, B.K.; Venkatesan, R.; Gawarkiewicz, G. Seasonal and tidal variability of surface currents in the Western Andaman Sea using HF radars and buoy observations during 2016–2017. *IEEE Transactions on Geoscience Remote Sensing* **2020**, *59*, 7235-7244. 608-610
17. Paduan, J.; Cook, M.; Fernandez, D. Two-dimensional diurnal to monthly period surface currents in Monterey Bay from CODAR-type HF radar. In Proceedings of the IGARSS'97. 1997 IEEE International Geoscience and Remote Sensing Symposium Proceedings. Remote Sensing-A Scientific Vision for Sustainable Development, 1997; pp. 1814-1816. 611-613
18. Gurgel, K.-W.; Antonischki, G.; Essen, H.-H.; Schlick, T. Wellen Radar (WERA): A new ground-wave HF radar for ocean remote sensing. *Coastal engineering* **1999**, *37*, 219-234. 614-615

19. Hammond, T.; Pattiaratchi, C.; Eccles, D.; Osborne, M.; Nash, L.; Collins, M.B. Ocean surface current radar (OSCR) vector measurements on the inner continental shelf. *Continental Shelf Research* **1987**, *7*, 411-431. 616
617
20. Emery, B.M.; Washburn, L.; Harlan, J.A. Evaluating radial current measurements from CODAR high-frequency radars with moored current meters. *Journal of Atmospheric Oceanic Technology* **2004**, *21*, 1259-1271. 618
619
21. Shen, Z.; Wu, X.; Lin, H.; Chen, X.; Xu, X.a.; Li, L. Spatial distribution characteristics of surface tidal currents in the southwest of Taiwan Strait. *Journal of Ocean University of China* **2014**, *13*, 971-978. 620
621
22. McMahon, T.; Raine, R.; Titov, O.; Boychuk, S. Some oceanographic features of northeastern Atlantic waters west of Ireland. *ICES Journal of Marine Science* **1995**, *52*, 221-232. 622
623
23. Pingree, R.; Griffiths, D. Currents driven by a steady uniform wind stress on the shelf seas around the British-Isles. *Oceanologica acta* **1980**, *3*, 227-236. 624
625
24. Pingree, R.; Le Cann, B. Three anticyclonic Slope Water Oceanic eDDIES (SWODDIES) in the southern Bay of Biscay in 1990. *Deep Sea Research Part A. Oceanographic Research Papers* **1992**, *39*, 1147-1175. 626
627
25. Polonsky, A.; Sukhonos, P. Variability of the wind stress, the field of currents, wind stress curl and vorticity of surface currents in the North Atlantic. *Izvestiya Rossiiskoi Akademii Nauk. Seriya Geograficheskaya* **2017**, 62-73. 628
629
26. Saviano, S.; Esposito, G.; Di Lemma, R.; de Ruggiero, P.; Zambianchi, E.; Pierini, S.; Falco, P.; Buonocore, B.; Cianelli, D.; Uttieri, M. Wind Direction Data from a Coastal HF Radar System in the Gulf of Naples (Central Mediterranean Sea). *Remote Sensing* **2021**, *13*, 1333. 630
631
632
27. Dobrynin, M.; Kleine, T.; Düsterhus, A.; Baehr, J. Skilful seasonal prediction of ocean surface waves in the Atlantic Ocean. *Geophysical Research Letters* **2019**, *46*, 1731-1739. 633
634
28. Gonzalez, P.L.; Brayshaw, D.J.; Zappa, G. The contribution of North Atlantic atmospheric circulation shifts to future wind speed projections for wind power over Europe. *Climate Dynamics* **2019**, *53*, 4095-4113. 635
636
29. Barrick, D. First-order theory and analysis of MF/HF/VHF scatter from the sea. *IEEE Transactions on Antennas Propagation* **1972**, *20*, 2-10. 637
638
30. O'Donncha, F.; Hartnett, M.; Nash, S.; Ren, L.; Ragnoli, E. Characterizing observed circulation patterns within a bay using HF radar and numerical model simulations. *Journal of Marine Systems* **2015**, *142*, 96-110. 639
640
31. Paduan, J.D.; Rosenfeld, L.K. Remotely sensed surface currents in Monterey Bay from shore - based HF radar (Coastal Ocean Dynamics Application Radar). *Journal of Geophysical Research: Oceans* **1996**, *101*, 20669-20686. 641
642
32. Kundu, P.K.; Blanton, J.O.; Janopaul, M.M. Analysis of current observations on the Georgia shelf. *Journal of Physical Oceanography* **1981**, *11*, 1139-1149. 643
644
33. Shen, Z.; Wu, X.; Fei, Y.; Xu, X.a.; Chen, X. Surface tidal currents in the open sea area to the east of the Zhoushan Islands measured with high frequency surface wave radar. *Acta Oceanologica Sinica* **2013**, *32*, 5-10. 645
646
34. Mooers, C.N.K. A technique for the cross spectrum analysis of pairs of complex-valued time series, with emphasis on properties of polarized components and rotational invariants *Deep Sea Research and Oceanographic Abstracts* **1973**, *20*, 1129-1141. 647
648
35. Gonella, J. A Rotary-component method for analysing meteorological and oceanographic vector time series. *Deep Sea Research and Oceanographic Abstracts* **1972**, *19*, 833-846. 649
650
36. Perkin, H. Inertial oscillations in the Mediterranean. *Deep Sea Research and Oceanographic Abstracts* **1972**, *19*, 289-296. 651
37. Gonella, J. A rotary-component method for analysing meteorological and oceanographic vector time series. In *Proceedings of the Deep Sea Research and Oceanographic Abstracts, 1972*; pp. 833-846. 652
653
38. Calman, J. On the interpretation of ocean current spectra, part II: Testing dynamical hypotheses. *Journal of Physical Oceanography* **1978**, *8*, 644-652. 654
655

39. Mooers, C.N. A technique for the cross spectrum analysis of pairs of complex-valued time series, with emphasis on properties of polarized components and rotational invariants. In Proceedings of the Deep Sea Research and Oceanographic Abstracts, 1973; pp. 1129-1141. 656
657
40. Perkins, H. Inertial oscillations in the Mediterranean. In Proceedings of the Deep Sea Research and Oceanographic Abstracts, 1972; pp. 289-296. 659
660
41. Pawlowicz, R.; Beardsley, B.; Lentz, S. Classical tidal harmonic analysis including error estimates in MATLAB using T_TIDE. *Computers Geosciences* **2002**, *28*, 929-937. 661
662
42. Halverson, M.; Pawlowicz, R. Tide, wind, and river forcing of the surface currents in the Fraser River plume. *Atmosphere-Ocean* **2016**, *54*, 131-152. 663
664
43. Arabelos, D.; Asteriadis, G.; Contadakis, M.; Spatalas, S.; Sachsamanoglou, H. Atmospheric tides in the area of Thessaloniki. *Journal of Geodynamics* **1997**, *23*, 65-75. 665
666
44. Leaman, K.D.; Sanford, T.B. Vertical energy propagation of inertial waves: A vector spectral analysis of velocity profiles. *Journal of Geophysical Research: Oceans* **1975**, *80*, 1975-1978, doi:<https://doi.org/10.1029/JC080i015p01975>. 667
668
45. Ren, L.; Yang, L.; Pan, G.; Zheng, G.; Zhu, Q.; Wang, Y.; Zhu, Z.; Hartnett, M.; 2022, Characterizing Residual Current Circulation and Its Response Mechanism to Wind at a Seasonal Scale Based on High-Frequency Radar Data, *14*, 4510 669
670
46. Li, R.; Chen, C.; Xia, H.; Beardsley, R.C.; Shi, M.; Lai, Z.; Lin, H.; Feng, Y.; Liu, C.; Xu, Q.; et al. Observed wintertime tidal and subtidal currents over the continental shelf in the northern South China Sea. *Journal of Geophysical Research: Oceans* **2014**, *119*, 5289-5310, doi:<https://doi.org/10.1002/2014JC009931>. 671
672
673
47. Yang, J.; Ding, W.; Cui, J.; Guo, S. Characteristical analysis of tidal and residual currents in the sea area around Tangshan international tourism island. *IOP Conference Series: Earth Environmental Science* **2021**, 632. 674
675
676